JACS Au
AN OPEN ACCESS JOURNAL OF THE AMERICAN CHEMICAL SOCIETY

pubs.acs.org/jacsau

Article

Optimally Selecting Photo- and Electrocatalysis to Facilitate CH_4 Activation on TiO_2(110) Surface: Localized Photoexcitation versus Global Electric-Field Polarization

Min Zhou and Haifeng Wang*

Cite This: *JACS Au* 2022, 2, 188–196

Read Online

ACCESS | Metrics & More | Article Recommendations | Supporting Information

ABSTRACT: Photo- and electrocatalytic technologies hold great promise for activating inert chemical bonds under mild conditions, but rationally selecting a more suitable method in between to maximize the performance remains an open issue, which requires a fundamental understanding of their different catalytic mechanisms. Herein, by first-principles calculations, we systematically compare the activation mechanisms for the C−H bond of the CH_4 molecule on TiO_2(110) under the photo- and electrocatalytic modes without or with water involved. It quantitatively reveals that the activation barrier of the C−H bond decreases dramatically with a surprising 74% scale by photoexcitation relative to that in thermocatalysis (1.12 eV), while the barrier varies with a maximum promotion of only 5% even under −1 V/Å external electric field (EEF). By detailed geometric/electronic analysis, the superior photocatalytic activity is traced to the highly oxidative lattice $O_{br}^{\bullet-}$ radical excited by a photohole (h^+), which motivates the homolytic C−H bond scission. However, under EEF from −1 V/Å to 1 V/Å, it gives a relatively mild charge polarization on the TiO_2(110) surface region and thus a limited promotion for breaking the weakly polar C−H bond. By contrast, in the presence of water, we find that EEF can facilitate CH_4 activation indirectly assisted by the surface radical-like OH* species from the oxidative water cleavage at high oxidative potential (>1.85 V vs SHE), which explains the high energy cost to drive electrocatalytic CH_4 conversion in experiment. Alternatively, we demonstrate that more efficient CH_4 activation could be also achieved at much lower oxidative potential when integrating the light irradiation. In such a circumstance, EEF can not only promote the h^+ accumulation at the catalyst surface but also help H_2O deprotonation to form hydroxide, which can serve as an efficient hole-trapper to generate $OH^{\bullet}$ radical ($OH^- + h^+ \rightarrow OH^{\bullet}$), unveiling an interesting synergistic photoelectrocatalytic effect. This work could provide a fundamental insight into the different characteristics of photo- and electrocatalysis in modulating chemical bond cleavage.

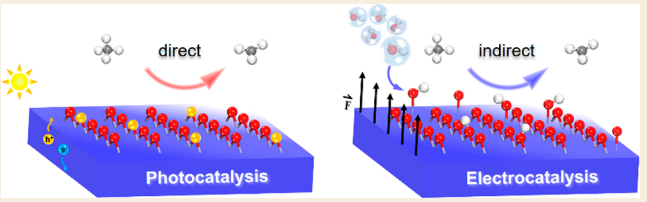

KEYWORDS: *density functional theory calculation, photocatalysis, electrocatalysis, CH_4 activation, electric-field effect, TiO_2*

INTRODUCTION

To achieve the efficient activation of inert C−H bond of methane (CH_4) at mild temperature is highly desired for facilitating the selective and controllable conversion of CH_4 into a value-added commodity, which constitutes one of the most fundamental and challenging tasks in the chemical community.[1−4] In this regard, the transition metal oxide (TMO) catalysts have drawn enormous attention in practice with the unsaturated metallic site and lattice oxygen exposed simultaneously;[5−7] particularly, the photo- and electrocatalytic technologies are recognized as promising approaches, with merits of altering reaction thermodynamics and kinetics under mild temperature driven by the external light and electricity energy supply. Significantly, some experiments have demonstrated the feasibility of photo- and electrocatalytic CH_4 conversion.[8−11] For example, Yoshida et al. reported that Pt/TiO_2 photocatalyst displayed high activity for CH_4 oxidation around room temperature (ca. 323 K).[12] The TiO_2 electrode decorated with RuO_2 and V_2O_5 was found capable of electrocatalytically converting CH_4 into methanol with a selectivity of 57% at an applied voltage of 2.25 V (vs standard hydrogen electrode, SHE).[13]

Despite these important findings, the insight into the activation of the first C−H bond in the CH_4 molecule under light irradiation and the electric-field (EF) polarization imposed by the cell potential has been not fully understood at the atomic level, which largely differs from the common thermocatalytic mode.[10,14] For example, qualitatively, the photoexcited polarons are believed to play an important role in the promotion effect with uncertainty. Wei et al.[15] proposed that the hole-trapped lattice oxygen radical was the main species for CH_4 activation over the β-Ga_2O_3 photocatalyst

Received: October 20, 2021
Published: December 22, 2021

https://doi.org/10.1021/jacsau.1c00466
JACS Au 2022, 2, 188–196

under 254 nm light irradiation, which was also suggested on other metal oxide catalysts such as Ag-decorated ZnO, $SrCO_3$/$SrTiO_3$, and so on.[16−18] However, the photoelectron could be also controversially responsible for the enhanced CH_4 activation at mild conditions.[19−21] Thus, a quantitative description of the activation process incorporating the kinetic barrier for CH_4 activation in the photocatalytic mode remains an unresolved essential issue.

Similar to the photocatalysis, the electrocatalytic approach is usually believed to be capable of modulating the chemical bond breaking/reforming through the EF effect,[22] but to our knowledge, how largely the EF polarization effect directly affects the C−H activation on the semiconductor is less understood, despite that some important progress on the EF tuning effect has been achieved on the transition metal catalysts (e.g., Ni, Pt, Co, and so on).[23−29] Moreover, as an extended fundamental question, one may also wonder: theoretically, which catalytic mode is more efficient in facilitating the C−H bond and other chemical bonds? Interestingly, the current research implies that the electrochemical oxidation of CH_4 appears to be kinetically slow and energy intensive.[30−33] For example, only when the applied potential (U_{app}) increases to 2.25 V (vs SHE) can the efficiency of electrocatalytic CH_4 conversion increase rapidly with a selectivity toward methanol reaching 57% over a TiO_2/RuO_2/V_2O_5 electrode; with a low U_{app} (<2.25 V), the improvement of the EF-imposed catalytic efficiency becomes relatively limited.[13,34] Remarkably, when combining the electrocatalytic condition with the light irradiation, the activation of CH_4 can occur on pure TiO_2 catalyst at a much reduced U_{app}; as shown from the experimental fact, the selectivity of CH_4 steam reforming toward CO reached up to 81.9% over TiO_2 surface under −0.41 V vs SHE.[9,35] Rationalizing these questions is not straightforward, and evidently, the photo- and electrocatalytic modes exhibit distinct catalytic characters. Some key questions are as follows: How does the EF imposed by the external voltage affect the C−H activation below and above 2.25 V (vs SHE) on TiO_2 catalysts? What are the unique characteristics of photo- and electrocatalysis, respectively? How can they cooperate with each other?

To quantitatively understand the photo- and electrocatalytic characteristics on CH_4 activation and rationalize their essential differences, here we carried out systematic DFT+U calculations with the PBE functional benchmarked against the advanced HSE06 hybrid functional for selected geometries on CH_4 activation over the rutile TiO_2(110) surface, a cross-sectional oxide support in photoelectrocatalytic reaction. The results unambiguously disclose and explain the unequivalent effects of light and electric field on CH_4 activation. Light irradiation can remarkably promote the C−H bond activation directly by the localized photogenerated hole, while the direct EF polarization effect on C−H cleavage in the electrochemical mode is unexpectedly weak. Mechanistically, we found that the C−H activation undergoes different mechanisms in diverse external driving forces. To activate the C−H bond on TiO_2(110), the electrochemical mode could have to indirectly make use of the radical-like OH* intermediate from environment H_2O dissociation via the proton coupled electron transfer (PCET) mechanism. Moreover, we also demonstrated that these two distinct function mechanisms of photocatalysis and electrocatalysis will give an improved activity when integrated cooperatively.

RESULTS AND DISCUSSION

Thermocatalytic Activation of CH_4

To begin with, the adsorption and activation of the CH_4 molecule on the TiO_2(110) surface in the thermocatalytic condition were first calculated as a benchmark. The rutile TiO_2(110) surface comprises two types of main active sites: the two-coordinated bridge oxygen and five-coordinated Ti cation (Figure 1a), denoted as O_{br} and Ti_{5c}, respectively.[36]

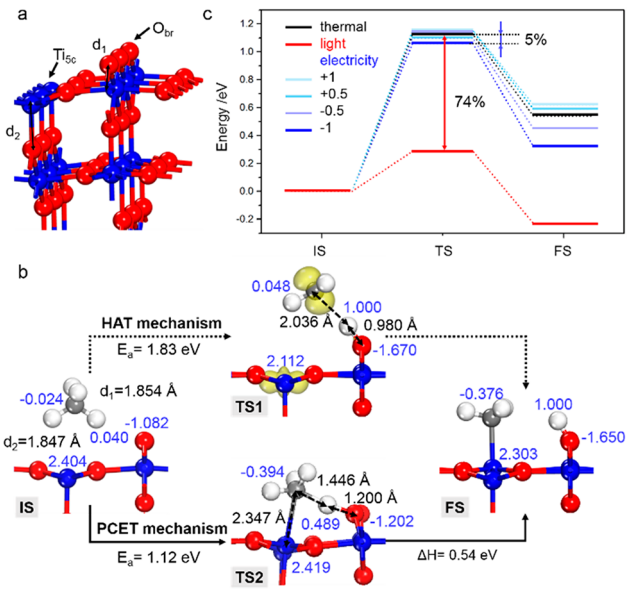

Figure 1. (a) Surface structure of optimized rutile TiO_2 (110), with the corresponding O−Ti bonds defined as d_1 and d_2. (b) Two possible mechanisms for CH_4 activation in thermocatalysis incorporating the spin density distributions of initial state (IS), transition state (TS), and final state (FS) at isovalue = 0.005. Some key bond lengths and Bader charges are marked in black and blue, respectively. Bader charge unit: lel. Red, blue, gray, and white balls represent O, Ti, C, and H atoms, respectively. These notations are used throughout the paper. (c) Energy profiles of CH_4 activation in three different external driving forces (light, electricity, and thermal energy).

Because of the geometrically high symmetry of the CH_4 molecule, it can weakly adsorb on the TiO_2(110) surface with an adsorption energy (E_{ads}) of −0.32 eV, wherein CH_4 interacts mainly with d_{z^2} orbital of the surface Ti_{5c} atom.[37,38] As the transition state (TS1) shows in Figure 1b, when C−H bond activation of CH_4 follows the homolytic cleavage mode at the O_{br} site (i.e., the so-called hydrogen atom transfer (HAT) mechanism),[6,39] it gives a reaction barrier as high as 1.83 eV, which corresponds to $CH_4 + Ti_{5c}^{4+} + O_{br}^{2-} \rightarrow CH_3^{\bullet} + Ti_{5c}^{3+} + O_{br}H^-$ with the $CH_3^{\bullet}$ radical formed and the released electron being trapped at Ti_{5c}^{4+} into Ti_{5c}^{3+} at TS1. By comparison, in response to the synergistic coupling of Ti_{5c}^{3+} with the $CH_3^{\bullet}$ radical, the C−H bond activation prefers to proceed via the proton coupled electron transfer (PCET) mechanism[40] ($CH_4 + Ti_{5c}^{4+} + O_{br}^{2-} \rightarrow Ti_{5c}^{4+}{-}CH_3^- + O_{br}H^-$, see TS2 in Figure 1b) at the Ti_{5c} and O_{br} dual sites with a lower barrier of 1.12 eV, which can be apparently taken as a heterolytic cleavage mechanism. Specifically, as the spin charge distribution of the transition state (TS2) illustrates in Figure 1b, the O_{br} site captures the dissociated hydrogen, and Ti_{5c} as a Lewis acidic center stabilizes the methyl group, yielding a proton and a methyl anion (corresponding to Bader charges of

https://doi.org/10.1021/jacsau.1c00466
JACS Au 2022, 2, 188−196

1.000 and −0.376 |e|, respectively), respectively. The forming H−O_{br} and C−Ti_{5c} bonds in the TS2 are measured to be 1.200 and 2.347 Å, respectively. Nevertheless, overcoming the activation barrier of 1.12 eV is kinetically difficult at room temperature, which accords with the fact that CH_4 activation generally has to be operated at high temperature.[41,42]

Photocatalytic Activation of CH_4

Under light irradiation, the photogenerated hole/electron pairs are generated and could be separated and localized at the different regions of the TiO_2(110) surface, where the photogenerated hole tends to be trapped by surface O_{br} to generate $O_{br}^{\bullet-}$ radical (i.e., $O_{br}^{2-} + h^+ \rightarrow O_{br}^{\bullet-}$), while the photogenerated electron can be localized at Ti_{5c}^{4+} to form the Ti_{5c}^{3+} radical (i.e., $Ti_{5c}^{4+} + e^- \rightarrow Ti_{5c}^{3+}$), which has been demonstrated in our previous studies and others.[43−45] As displayed in Figure S1, with the assistance of Ti_{5c}^{3+}, the barrier of CH_4 activation is decreased a little to 0.99 eV with the strengthened stabilization of the CH_3 intermediate by the Ti_{5c}^{3+} site, and the reaction behavior is the same as that in thermocatalysis with a similar TS structure (see in Figure S1). Interestingly, in the presence of $O_{br}^{\bullet-}$ radical, the barrier of C−H bond cleavage of the CH_4 molecule (i.e., $CH_4 + O_{br}^{\bullet-} \rightarrow HO_{br}^{-} + CH_3^{\bullet}$) can be greatly reduced to as low as 0.29 eV (see energy profile in Figure 1c). In comparison with the thermocatalytic case, the promotion scale of the activation barrier is quantitatively estimated to be an order of 74% (0.29 eV versus 1.12 eV). One can thus anticipate that the photocatalytic conversion would be an efficient way for activating CH_4 on TiO_2(110) if there are sufficient surface $O_{br}^{\bullet-}$ species by increasing light absorption and decreasing the recombination of hole/electron pairs.

By analyzing the geometric/electronic structure of the resulting TS (Figure 2), one can see that the C−H cleavage

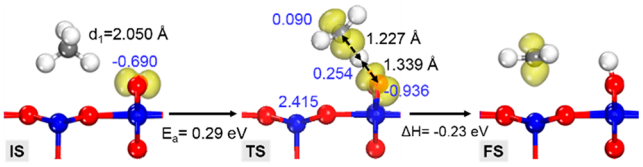

Figure 2. Geometry structures and spin density distributions of IS, TS, and FS for CH_4 activation on TiO_2(110) with the assistance of photogenerated hole.

mode changes evidently owing to the participation of $O_{br}^{\bullet-}$ species; specifically, the TS changes from the original dihapto configuration (with the CH_3 and H atom in CH_4 bonded to the Lewis acid/base site, Ti_{5c}/O_{br}, respectively) in the thermocatalytic case to the monohapto configuration, in which the H atom is captured by the $O_{br}^{\bullet-}$ site and the methyl radical suspends above the TiO_2 surface. The bond lengths of the CH_3···H and H···O_{br} in the TS are 1.227 and 1.339 Å, respectively. In other word, it exhibits a radical-like TS type, and the radical nature of CH_3 species is also confirmed by a Bader charge of 0.090 |e| and a magnetic moment of 0.43 μ_B (Table S3). Therefore, the C−H bond activation modulated by the photoexcited hole essentially follows a homolytic cleavage mechanism or the so-called hydrogen-atom transfer mechanism.[40]

In addition, by analyzing the Bader charge of the $O_{br}^{\bullet-}$ center, it is found that it holds less electron than the O_{br}^{2-} site in thermocatalysis (−0.690 vs −1.082 |e|). In this sense, we can rationalize that the $O_{br}^{\bullet-}$ center, as a strong oxidative site with an unoccupied 2*p* orbital, can more easily capture electrons from the dissociated hydrogen atom than O_{br}^{2-}, thereby leading to a much decreased barrier of C−H bond activation. By contrast, in the thermocatalytic condition, the oxidizability of the close-shell O_{br}^{2-} is too weak to break the strong C−H bond in the CH_4 molecule.

Electrocatalytic Activation of CH_4

As a quantitative comparison, the adsorption and activation of CH_4 in a series of electric-field intensities (−1 V/Å ≤ *F* ≤ 1 V/Å) were calculated and are shown in Table 1. When the negative EEFs are applied, the CH_4 adsorption and activation progresses can be facilitated. For example, in comparison with the zero EEF, the adsorption energy of CH_4 at −1 V/Å increases from −0.32 eV to −0.41 eV, and the CH_4 activation barrier deceases from 1.12 to 1.06 eV (Figure 3a). However, to our surprise, the contribution of EEFs on CH_4 activation is relatively weak (on an order of only 5% in −1 V/Å relative to that in 0 V/Å), whereas the positive EEFs suppress this progress. Specifically, the activation barrier increases gradually with the increasing of the applied electric fields from −1 V/Å to 1 V/Å (Figure 3b). Moreover, by fitting the activation barriers (E_a) versus the EEF intensities (*F*), we can obtain two independent linear relations with different slopes in the negative and positive EEF regions:

$$E_a = 0.07 \times F + 1.13 \quad (\text{when } -1\ \text{V/Å} \le F < 0\ \text{V/Å})$$

$$E_a = 0.03 \times F + 1.13 \quad (\text{when } 0\ \text{V/Å} \le F \le 1\ \text{V/Å})$$

Obviously, the slope in negative EEFs is more than twice than that in positive EEFs, indicating that the negative EFs possess a more sensitive influence on promoting the CH_4 activation progress. Furthermore, it is worth noting that the

Table 1. Adsorption Energies of the CH_4 Molecule on the TiO_2(110) Surface (E_{ads}), as well as the Activation Barriers (E_a) and Enthalpy Changes (ΔH) of CH_4 Activation, and the Optimized Average O−Ti bond lengths (d_1 and d_2), Bader Charges of O_{br} and Ti_{5c} Sites, and -ICOHP Values of C−Ti_{5c} and H−O_{br} Bonds in TSs, Obtained in Different EEFs (F) Using DFT+U

				bond length		Bader charge		-ICOHP (eV)	
EEF (V/Å)	E_{ads} (eV)	E_a (eV)	ΔH (eV)	d_1 (Å)	d_2 (Å)	O_{br}	Ti_{5c}	C−Ti_{5c}	H−O_{br}
−1.00	−0.41	1.06	0.32	1.840	1.863	−1.048	2.432	1.516	2.452
−0.50	−0.35	1.10	0.45	1.846	1.854	−1.066	2.434	1.409	2.465
−0.35	−0.35	1.11	0.48	1.848	1.853	−1.066	2.409	1.391	2.468
0.00	−0.32	1.12	0.54	1.854	1.847	−1.082	2.404	1.341	2.468
0.35	−0.27	1.14	0.57	1.859	1.841	−1.094	2.405	1.246	2.463
0.50	−0.24	1.15	0.59	1.860	1.838	−1.114	2.402	1.216	2.471
1.00	−0.18	1.15	0.62	1.868	1.831	−1.135	2.397	1.113	2.482

https://doi.org/10.1021/jacsau.1c00466
JACS Au 2022, 2, 188−196

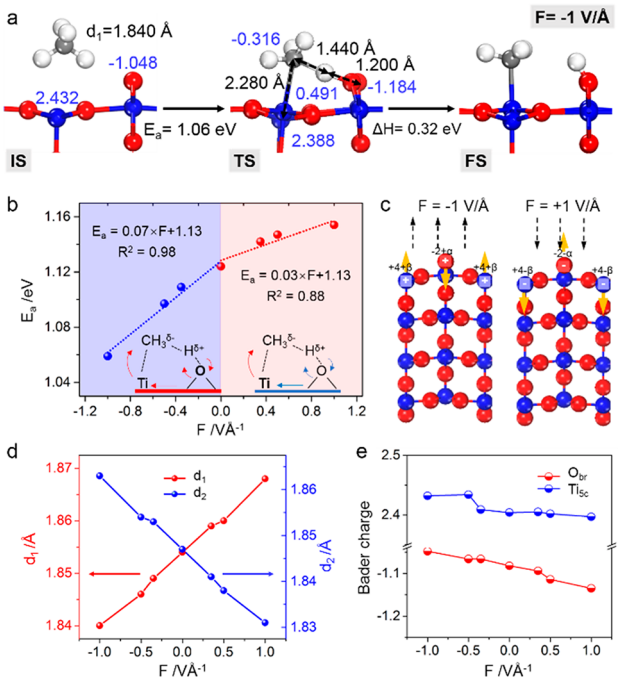

Figure 3. (a) Structures and spin density distributions of IS, TS, and FS for CH_4 activation at −1 V/Å. (b) Correlations between E_a and F, as well as the mechanism schemes for CH_4 oxidation modulated by negative (left) and positive (right) EEFs, in which red arrows indicate the promotion effect, whereas blue arrows signify the suppression effect. (c) Schematic diagram for surface charge polarization and atomic fluctuation at different EEFs. (d, e) Bond length changes of d_1 and d_2, as well as Bader charge changes of O_{br} and Ti_{5c} versus F.

C−H bond dissociation mechanism under EEF is the same as that in thermocatalytic conditions, maintaining a two-site assisted TS configuration. Taking the reaction in −1 V/Å as an example, the $CH_3\cdots Ti_{5c}$ bond is 2.280 Å, which is slightly shorter than that without the EF effect (2.347 Å). Additionally, the changes of $CH_3\cdots H$ and $O_{br}\cdots H$ bonds are also tiny (1.440 vs 1.446 Å and 1.200 vs 1.200 Å, respectively, Figure 3a).

Origins behind the Differences between Photo- and Electro-catalysis

Intuitively, the electrocatalytic approach is similar to photocatalysis, except for the energy source which comes from EEFs.[46] However, why are the EEFs far less efficient than light irradiation on CH_4 activation, and how do the EEFs affect the CH_4 activation progress? To solve these puzzles and unveil the inherent mechanisms of EEF and light on CH_4 activation, the geometric and electronic structure analyses on TiO_2(110) catalyst under different external driving forces were carried out.

First, the structural responses and charge states of O_{br} and Ti_{5c} sites, as the main reactive centers on TiO_2(110), were investigated. In photocatalysis, the hole activated O_{br} and electron activated Ti_{5c} are featured with an obvious extension of O_{br}−Ti and Ti_{5c}−O bonds (denoted as d_1 and d_2 in Figure 1a, respectively) by 0.196 and 0.205 Å, respectively (Figures 1b and 2).[36,47] Interestingly, under different EEFs from 1 V/Å to −1 V/Å, we found that the d_2 increased, whereas the d_1 decreased gradually (see Table 1 and Figure 3d), with the increment (decrement) magnitude of d_2 (d_1) being only 0.03 Å. Noteworthily, this finding seems to be contrary to our general cognition that, with the negative EEF imposed (corresponding to the oxidative potential), the surface is polarized to be electron-deficient (Figure 3c), which is favorable to the activation of O_{br}, and d_1 should be elongated compared to the inactivated ones.

To shed light on these different behaviors, we conducted the detailed electronic structure analysis, including plane-averaged electrostatic potential (PAEP) distribution and Bader charge analysis. As illustrated in Figure S2 for the PAEPs of the TiO_2(110) surface under different EEFs, the main difference of

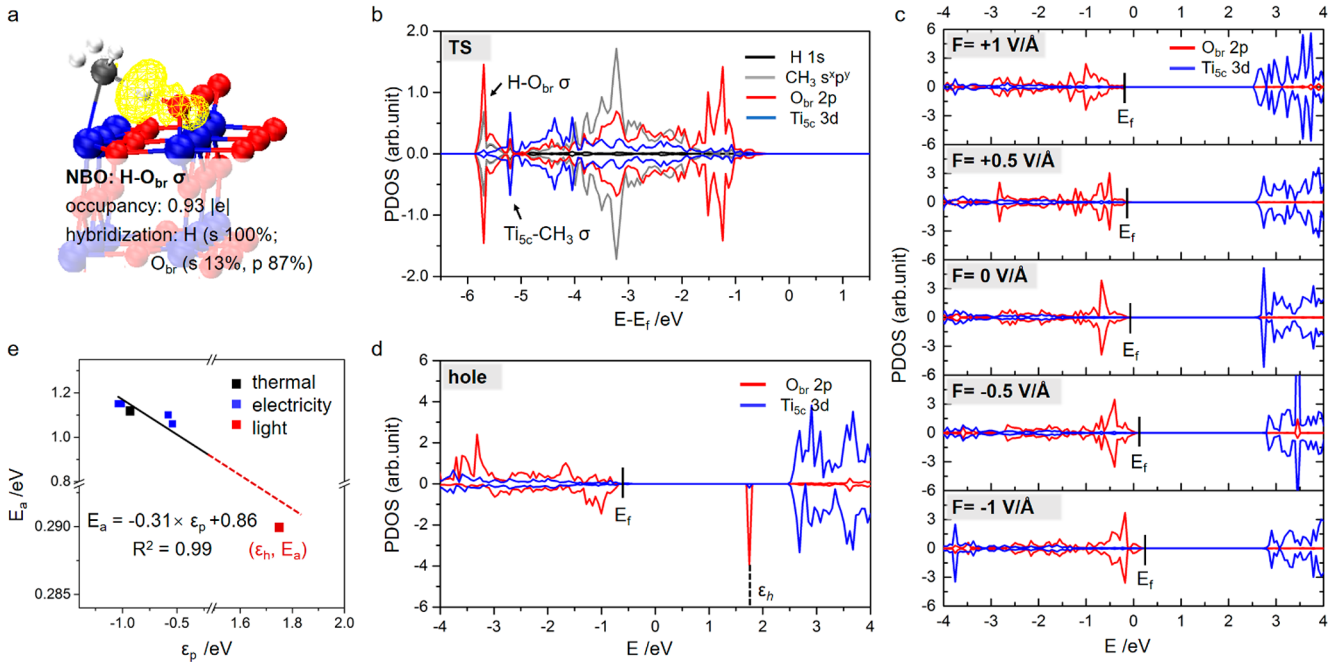

Figure 4. (a) NBOs and (b) projected density of state (PDOS) of the TS for CH_4 activation on TiO_2(110) in thermal conditions. (c, d) PDOSs of O_{br}-2*p* and Ti_{5c}-3*d* bands of the bare surface in different EEFs and light, respectively. (e) Correlation between CH_4 activation barrier (E_a) and *p*-band center (ε_p) of the O_{br} site in EEFs (or energy level of characteristic peak of the hole localization, ε_h, in light).

https://doi.org/10.1021/jacsau.1c00466
JACS Au 2022, 2, 188−196

electrostatic potential appears at the surface region and above, indicating the relatively stronger polarization of EEF on the catalyst surface than in the bulk. Nevertheless, by Bader charge analysis on surface atoms (Figure 3e and Table 1), we found that the most negative EEF (−1 V/Å) only led to a small fraction of charge depletion for both O_{br} and Ti_{5c} atoms, which existed as $O_{br}^{-2+\alpha}$ and $Ti_{5c}^{+4+\beta}$ ($0 < \alpha, \beta \ll 1$), respectively. Thus, we can deduce that the electronic field line interacts weakly with groups of positively charged Ti_{5c} and negatively charged O_{br} atoms, respectively, and relaxes themselves along the electronic field line to minimize the potential energy, which contributes to the weak fluctuation of surface atoms, i.e., the decrement/increment of d_1/d_2 (see the illustration in Figure 3c). This is different from the photocatalytic mechanism: accompanying the localization of a photoexcited hole on O_{br}, the interaction between this specific hole-trapped O_{br} and substrate is strongly weakened, and the charge changes a lot from −1.082 |e| to −0.690 |e|, which is much larger than the effect of EEF.

Second, with the above basic understandings, we are now at the position to discuss why the barrier of CH_4 activation in positive EEF increases much slower than that in negative EEF, as Figure 3b shows. The periodic natural bond orbital (NBO) analysis[48,49] was performed to show the bonding nature of two-site assisted TS complex in thermocatalysis. As can be seen from the H−O_{br} NBOs in Figure 4a (with details labeled), the H−O_{br} σ bond is largely composed of the hydrogen *s* orbital and oxygen *p* orbitals, which corresponds to the characteristic peak at the energy level of −5.70 eV from the PDOS of TS (Figure 4b). Noticeably, a tiny characteristic peak of the Ti_{5c}−CH_3 σ bond appears below the Fermi level at the energy level of −5.20 eV with an extremely small occupied area of only 0.008 |e|, which implies a weak C−Ti_{5c} bond. One can thus speculate that the activation of CH_4 depends mainly on the reactivity of the O_{br} site, whereas the Ti_{5c} site contributes secondarily. The higher value of integrated crystal orbital Hamilton population (-ICOHP)[50] on the H−O_{br} (2.468 eV/bond) than that on the C−Ti_{5c} bond (1.341 eV/bond) confirms this speculation (see Table 1). Thus, the observation that a smaller slope exists in positive EEFs can be explained. When the positive EEF is exposed, the surface is in an electron-rich state, which reduces the reactivity of the O_{br} site for accepting H; simultaneously, the Ti_{5c} site, as a secondary reaction site, is activated and facilitates binding with the CH_3 group, thus leading to an overall slow increment of reaction barrier with the increment of positive EEFs (see inserted mechanism scheme in Figure 3b). By contrast, the O_{br} is activated while Ti_{5c} is inactivated in the negative EFF, and a relatively larger variation of the reaction barrier can be expected.

Third, we did the orbital-projected densities of state (PDOS) of surface O_{br}-2*p* and Ti_{5c}-3*d* bands, which determined the reactivity of the catalyst, to uncover the reactivity trends of photo/electro- versus thermocatalysis. As illustrated in Figure 4c, with the decrement of EEFs from 1 V/Å to −1 V/Å, the energy level of the O_{br}-2p band (constituting the valence band maximum, VBM) up-shifts gradually, which indicates a better oxidizability of the O_{br} site to accept the H atom by forming the polar covalent H−O_{br} bond. Quantitatively, we calculated the occupied p-band center (ε_p) of O_{br} site, an important indicator to describe the reactivity of the reaction center. The ε_p of the catalyst in different EEFs (+1, +0.5, 0, −0.5, and −1 V/Å) were calculated to be −1.04, −1.01, −0.93, −0.58, and −0.54 eV, respectively, confirming that negative EEFs result in the upshifting of the p-band center of the O_{br} site. Remarkably, a linear correlation between the activation barriers (E_a) and ε_p exists (Figure S3), implying that the upshifting of the EEF-induced p-band mainly accounts for the decrement of CH_4 activation barrier on TiO_2(110) surface.

In the presence of the photoinduced hole, by analyzing the PDOS in Figure 4d, we found that the formation of $O_{br}^{\bullet-}$ radical introduced a localized paramagnetic state (1.75 eV above the Fermi level) in the band gap, manifesting itself in the large upward shift relative to the VBM. The localized paramagnetic hole state serves as a springboard to accommodate the released electron from CH_4 dissociation (i.e., $CH_4 + O_{br}^{\bullet-} \rightarrow HO_{br}^{-} + CH_3^{\bullet}$), which is characterized with an extremely strong oxidative ability to facilitate CH_4 activation. Interestingly, the decreased E_a with the high-energy-level $O_{br}^{\bullet-}$ characteristic peak (1.75 eV) can be also well fitted in the linear correlation between E_a and ε_p in EEFs (Figure 4e).

Based on these computational results, a picture for CH_4 activation on the TiO_2(110) surface in different external fields can be proposed. Upon introducing negative/positive EEFs, the 2*p*-bands of all the surface O_{br} sites are polarized to a higher/lower energy level, which enhances/depresses the activation of CH_4. Similarly, for CH_4 activation in light illumination, the unoccupied 2*p* hole state is the key for surging the catalytic activity. More specifically, the origins behind the superior performance of light than electricity could be understood. In photocatalysis, photogenerated carriers are quantized. These holes activate surface individual lattice oxygen to form $O_{br}^{\bullet-}$ radicals, which have a strong oxidizability, whereas for electrocatalysis, groups of surface lattice oxygens are influenced gently by the electronic field line owing to the strong Ti−O chemical bond, which contributes to upshift of 2*p*-band and thereby prompts oxidizability of the O_{br} site on CH_4 activation.

Since the EEFs have a weak contribution to the direct CH_4 activation by the TiO_2(110) catalyst, one may naturally question the two experimental results mentioned above that (i) the kinetics of electrocatalytic CH_4 steam reforming can be accelerated over the TiO_2-based electrode, when the potential is above 2.25 V (vs SHE),[13] and (ii) when combining the electrocatalytic condition with the light irradiation, the activation of CH_4 can occur even on pure TiO_2 catalyst with a much reduced voltage (−0.41 V vs SHE).[35] Considering that the H_2O molecule, as the main medium in electrocatalysis and photoelectrocatalysis systems, may have some indispensable roles on CH_4 conversion via the dissociated reactive oxygen species, we examined the electrocatalytic H_2O dissociation and CH_4 activation to answer these two questions.

First, the oxidative water cleavage via the proton coupled electron transfer (PCET) process was tested, including (i) $H_2O + * \rightarrow OH^* + H^+ + e^-$ and (ii) $OH^* \rightarrow O^* + H^+ + e^-$, where * denotes Ti_{5c}.[51] Following this path, the formed surface OH* and O* intermediate would be radical-like, evidenced with Bader charges of −0.011 |e| and −0.014 |e| on TiO_2(110) surface, respectively. Remarkably, our calculations uncover that the OH* and O* species can facilitate CH_4 activation greatly with much lower barriers of 0.36 and 0.45 eV, respectively (Figure 5a). However, this PCET process is thermodynamically difficult to occur, which has to be driven by high oxidative potential. Specifically, the thermodynamic stability of the surface OH*/O* as a function of the applied potential *U* at pH = 7 is presented in Figure 5b (see details in Table S4). We can

https://doi.org/10.1021/jacsau.1c00466
JACS Au 2022, 2, 188−196

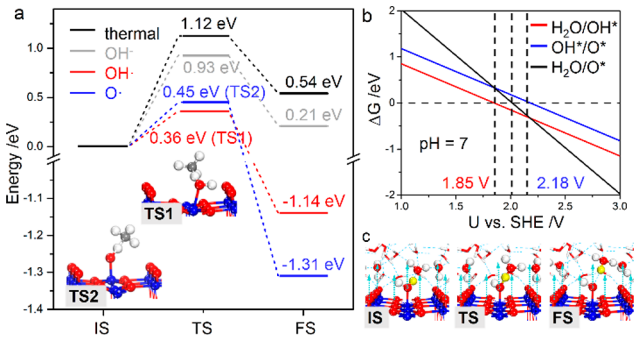

Figure 5. (a) Optimized TSs and barriers for CH_4 activation with the assistance of $OH^{\bullet}/O^{\bullet}$ species from H_2O dissociation via PCET and OH^- intermediate via PT progress, respectively. (b) Thermodynamic phase diagram of H_2O conversion on $TiO_2(110)$ as a function of the potential at the pH = 7, including (i) $H_2O + * \rightarrow OH^* + H^+ + e^-$ (red), (ii) $OH^* \rightarrow O^* + H^+ + e^-$ (blue), and (iii) $H_2O + * \rightarrow O^* + 2H^+ + 2e^-$ (black). (c) Geometries of PT progress for H_2O dissociation with the proton released into the liquid phase.

see that only when the potential increases to 1.85 V, the OH* intermediate becomes thermodynamically favored to be formed; when the potential continues to increase to 2.18 eV, the O* begins to be formed. This accords with the electrocatalytic CH_4 steam reforming experiment over $TiO_2/RuO_2/V_2O_5$ electrode that CH_4 can be activated when the applied potential is above 2.25 V (vs SHE)[13,34] and is also arguably in line with the observation that hydroxide and oxygen adatoms are produced on Ti_{5c} sites under a voltage pulse of 2.4 or 2.8 V on the $TiO_2(110)$ surface.[52]

Thus, we can comprehend that the EEF effect at high oxidative potential can hardly activate CH_4 directly but could alternatively activate CH_4 (when H_2O exists) by resorting to the surface active species (i.e., OH*) from the oxidative water cleavage indirectly. In addition, it may be worth noting that the applied potential is better when it is not higher than 2.18 V, as the reactive O* species can not only facilitate CH_4 activation (E_a = 0.45 eV, Figure 5a) but also simultaneously promote oxygen evolution via O−O coupling.[47] This is in line with the experimental observation over the $TiO_2/RuO_2/V_2O_5$ electrode, that the CH_4 oxidation process is prompted below 2.25 V (vs SHE) but is inhibited at a more positive potential with simultaneous oxygen evolution.[13]

Second, the dissociation of water via the deprotonation progress (i.e., proton-transfer mechanism, PT) into the solution was comparatively calculated at the $H_2O/TiO_2(110)$ interface by the ab initio molecular dynamics (AIMD) simulation[53] (see method details in Supporting Information), which corresponds to $Ti_{5c}-H_2O \rightarrow Ti_{5c}-OH^- + H^+$ (Figure 5c). In comparison with the PCET process, this PT process occurs relatively easily with a low barrier of 0.39 eV and reaction enthalpy of 0.21 eV at the thermal condition. Furthermore, our calculations verified that the potential-induced EF effect would efficiently affect these proton transfer kinetics to form OH^- species. Specifically, the negative EFs (corresponding to the oxidative potential) lead to an evident promotional effect on H_2O dissociation (Table S5), resulting from the dipole moment and large polarizability of the O−H bond;[54] for example, there is a much decreased barrier of 0.08 eV at −1 V/Å. It implies that a low potential could be strong enough to facilitate the hydroxide OH^- formation. However, different from the radical-like OH* species in PCET progress, the formed OH^- can hardly facilitate CH_4 activation with a high barrier of 0.93 eV, which is comparable with the pristine inert O_{br} (1.12 eV, Figure 5a). Thus, the charge state of the OH intermediate on $TiO_2(110)$ is critical for modulating its reactivity.

Significantly, when integrating with the light irradiation (see schematic in Figure 6), the hydroxide OH^- generated under

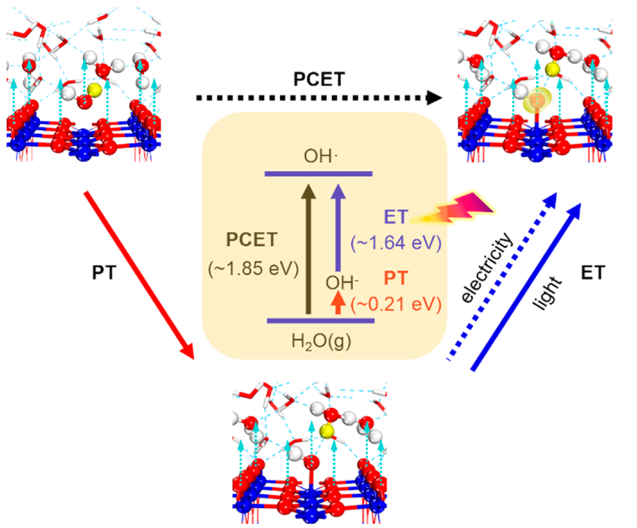

Figure 6. Schematic diagram for $OH^{\bullet}$ formation via PCET and PT +ET progresses. PCET: $H_2O^* \rightarrow OH^{\bullet} + H^+ + e^-$; PT: $H_2O^* \rightarrow OH^- + H^+$; and ET: $OH^- \rightarrow OH^{\bullet} + e^-$. Note: 1.64 eV for ET progress; see details in Figure S6.

low potential (or low EEF) could bring about an evident synergy effect for CH_4 activation. Under a pure photocatalytic condition, it was reported to be only a H_2O dissociation probability of about 1.7% and 3.7% on $TiO_2(110)$ at the 400 and 355 nm light irradiation, respectively,[52] largely restricted by the high recombination rate of the photoexcited electron−hole (namely, the low concentration of the surface hole)[20,55] and relatively low kinetics of H_2O photocatalytic oxidation progress (i.e., $H_2O + h^+ \rightarrow OH^{\bullet} + H^+$).[36,47] However, with the cooperation of photo- and electrocatalysis, the photohole can readily trap the OH^- species (i.e., $OH^- + h^+ \rightarrow OH^{\bullet}$) generated from electrocatalysis-accelerated H_2O deprotonation progress with a hole-trapping capacity of −0.77 eV,[36] to form $OH^{\bullet}$ radical for better CH_4 activation. In this sense, one can rationalize that, experimentally, just a low oxidative potential is required to accomplish the efficient CH_4 activation when combining with the photocatalysis.[35] In addition, our calculations identify that the imposed negative EEF under the oxidative potential can also enhance the direct distribution of hole/electron along/against the electric-field line, with the hole polaron being preferentially accumulated at the catalyst surface (see details in the Supporting Information, Figures S4 and S5).[56] Accordingly, the synergistic effect of photo-electrocatalysis can be further enhanced for motivating the formation of reactive $OH^{\bullet}$ radical. It may be worth noting that this finding could also explain the experimental phenomenon that the amount of O_2 increases with the increasing of EEFs in photoelectrocatalysis.[35]

In brief, the above discussions indicate that the electrocatalytic CH_4 conversion eventually needs to indirectly resort to the reactive oxygen species (e.g., $OH^{\bullet}$ radical). As Figure 6 illustrates, the formation of $OH^{\bullet}$ radical can be accomplished

https://doi.org/10.1021/jacsau.1c00466
JACS Au 2022, 2, 188−196

from the oxidative cleavage of H_2O via the PCET mechanism; however, the required applied oxidative potential is rather high. Alternatively, $OH^•$ could be formed via the sequential PT+ET processes, during which the PT process occurs relatively easily kinetically on $TiO_2(110)$ and can be efficiently modulated by the low EEF, whereas the ET process is energy-intensive with an energy cost over 1.64 eV (see details in Figure S6). In this circumstance, the light irradiation could be a competent approach to surmount this high energy demand and drive this ET process ($OH^- + h^+ \rightarrow OH^•$). In this regard, the integrated photoelectrochemical strategy should be promising for achieving efficient CH_4 activation.

CONCLUSIONS

In summary, the present study provides a comprehensive comparison between the photo- and electrocatalysis and uncovers their critical roles and unique mechanisms for modulating CH_4 oxidation by $TiO_2(110)$ in the absence or presence of water. It turns out that a positively polarized surface is helpful for CH_4 activation, whereas the contribution is largely inferior to a photogenerated hole in photocatalysis. The origins behind it were revealed: the negative EEFs contribute to the O_{br}-2*p* band upshift slightly toward the Fermi level, indicating the more reactivity of lattice oxygen to make a bond with H atom. For comparison, the photocatalysis reaction proceeds with the assistance of a localized gap state as a springboard, whose oxidizing ability is largely greater than that of the electro-activated lattice oxygen. Differently, the essential role of EEFs on CH_4 conversion on $TiO_2(110)$ can be strengthened in the presence of water. EEF can trigger the oxidative water cleavage via the PCET process under high oxidative potential, resulting in the formation of OH* radical-like species, which are reactive for CH_4 activation. Alternatively, EEF can facilitate H_2O deprotonation via the PT mechanism to form the surface hydroxide OH^-, which can easily trap the photoexcited hole to generate $OH^•$. In addition, it can also will promote the carrier spatial separation by stabilizing the hole−polaron configuration along the electric-field line in photoelectrocatalalysis, rationalizing the synergistic photoelectrocatalytic effect for boosting CH_4 activation on $TiO_2(110)$ at low applied potential.

ASSOCIATED CONTENT

Supporting Information

The Supporting Information is available free of charge at https://pubs.acs.org/doi/10.1021/jacsau.1c00466.

DFT setting details; calculations of free energy; promotion effect of EEF on the separation of carriers; test on the CH_4 activation barrier via DFT+U versus HSE06 functional; reaction barrier of H_2O deprotonation under different EEFs; optimized geometries and spin density plots for CH_4 activation assisted photogenerated electron; and the plane-averaged electrostatic potential of $TiO_2(110)$ under different EEFs (PDF)

AUTHOR INFORMATION

Corresponding Author

Haifeng Wang − *Key Laboratory for Advanced Materials, Centre for Computational Chemistry and Research Institute of Industrial Catalysis, East China University of Science and Technology, Shanghai 200237, China;* orcid.org/0000-0002-6138-5800; Email: hfwang@ecust.edu.cn

Author

Min Zhou − *Key Laboratory for Advanced Materials, Centre for Computational Chemistry and Research Institute of Industrial Catalysis, East China University of Science and Technology, Shanghai 200237, China*

Complete contact information is available at: https://pubs.acs.org/10.1021/jacsau.1c00466

Notes

The authors declare no competing financial interest.

ACKNOWLEDGMENTS

This project was supported by National Key R&D Program of China (2021YFA1500700), NSFC (21873028, 91945302,92045303), National Ten Thousand Talent Program for Young Top-notch Talents in China, Shanghai Shu-Guang project (17SG30), and the Fundamental Research Funds for the Central Universities

REFERENCES

(1) Sushkevich, V. L.; Palagin, D.; Ranocchiari, M.; van Bokhoven, J. A. Selective anaerobic oxidation of methane enables direct synthesis of methanol. *Science* **2017**, *356*, 523−527.

(2) Liu, Z.; Huang, E.; Orozco, I.; Liao, W.; Palomino, R. M.; Rui, N.; Duchon, T.; Nemsak, S.; Grinter, D. C.; Mahapatra, M.; Liu, P.; Rodriguez, J. A.; Senanayake, S. D.; et al. Water-promoted interfacial pathways in methane oxidation to methanol on a CeO_2-Cu_2O catalyst. *Science.* **2020**, *368*, 513−517.

(3) Laudadio, G.; Deng, Y.; van der Wal, K.; Ravelli, D.; Nuño, M.; Fagnoni, M.; Guthrie, D.; Sun, Y.; Noël, T. C (sp^3)−H functionalizations of light hydrocarbons using decatungstate photocatalysis in flow. *Science* **2020**, *369*, 92−96.

(4) Hu, A.; Guo, J. J.; Pan, H.; Zuo, Z. Selective functionalization of methane, ethane, and higher alkanes by cerium photocatalysis. *Science* **2018**, *361*, 668−672.

(5) Liang, Z.; Li, T.; Kim, M.; Asthagiri, A.; Weaver, J. F. Low-temperature activation of methane on the $IrO_2(110)$ surface. *Science* **2017**, *356*, 299−303.

(6) Latimer, A. A.; Kulkarni, A. R.; Aljama, H.; Montoya, J. H.; Yoo, J. S.; Tsai, C.; Abild-Pedersen, F.; Studt, F.; Norskov, J. K. Understanding trends in C-H bond activation in heterogeneous catalysis. *Nat. Mater.* **2017**, *16*, 225−229.

(7) Aljama, H.; Nørskov, J. K.; Abild-Pedersen, F. Theoretical Insights into Methane C−H Bond Activation on Alkaline Metal Oxides. *J. Phys. Chem. C* **2017**, *121*, 16440−16446.

(8) Kaliaguine, S. L.; Shelimov, B. N.; Kazansky, V. B. Reactions of methane and ethane with hole centers O^-. *J. Catal.* **1978**, *55*, 384−393.

(9) Song, H.; Meng, X.; Wang, Z. J.; Liu, H.; Ye, J. Solar-Energy-Mediated Methane Conversion. *Joule.* **2019**, *3*, 1606−1636.

(10) Meng, X.; Cui, X.; Rajan, N. P.; Yu, L.; Deng, D.; Bao, X. Direct Methane Conversion under Mild Condition by Thermo-, Electro-, or Photocatalysis. *Chem.* **2019**, *5*, 2296−2325.

(11) Bagherzadeh Mostaghimi, A. H.; Al-Attas, T. A.; Kibria, M. G.; Siahrostami, S. A review on electrocatalytic oxidation of methane to oxygenates. *J. Mater. Chem. A* **2020**, *8*, 15575−15590.

(12) Yoshida, H.; Hirao, K.; Nishimoto, J. I.; Shimura, K.; Kato, S.; Itoh, H.; Hattori, T. Hydrogen production from methane and water on platinum loaded titanium oxide photocatalysts. *J. Phys. Chem. C* **2008**, *112*, 5542−5551.

(13) Rocha, R. S.; Reis, R. M.; Lanza, M. R. V.; Bertazzoli, R. Electrosynthesis of methanol from methane: The role of V_2O_5 in the

reaction selectivity for methanol of a $TiO_2/RuO_2/V_2O_5$ gas diffusion electrode. *Electrochim. Acta* **2013**, *87*, 606−610.
(14) Zhao, Y.; Gao, W.; Li, S.; Williams, G. R.; Mahadi, A. H.; Ma, D. Solar- versus Thermal-Driven Catalysis for Energy Conversion. *Joule.* **2019**, *3*, 920−937.
(15) Wei, J.; Yang, J.; Wen, Z.; Dai, J.; Li, Y.; Yao, B. Efficient photocatalytic oxidation of methane over β-Ga_2O_3/activated carbon composites. *RSC Adv.* **2017**, *7*, 37508−37521.
(16) Chen, X.; Li, Y.; Pan, X.; Cortie, D.; Huang, X.; Yi, Z. Photocatalytic oxidation of methane over silver decorated zinc oxide nanocatalysts. *Nat. Commun.* **2016**, *7*, 12273.
(17) Pan, X.; Chen, X.; Yi, Z. Photocatalytic oxidation of methane over $SrCO_3$ decorated $SrTiO_3$ nanocatalysts via a synergistic effect. *Phys. Chem. Chem. Phys.* **2016**, *18*, 31400−31409.
(18) Schwach, P.; Pan, X.; Bao, X. Direct Conversion of Methane to Value-Added Chemicals over Heterogeneous Catalysts: Challenges and Prospects. *Chem. Rev.* **2017**, *117*, 8497−8520.
(19) Gondal, M. A.; Hameed, A.; Yamani, Z. H.; Arfaj, A. Photocatalytic transformation of methane into methanol under UV laser irradiation over WO_3, TiO_2 and NiO catalysts. *Chem. Phys. Lett.* **2004**, *392*, 372−377.
(20) Yuliati, L.; Yoshida, H. Photocatalytic conversion of methane. *Chem. Soc. Rev.* **2008**, *37*, 1592−1602.
(21) Shen, J.; Li, Z. J.; Hang, Z. F.; Xu, S. F.; Liu, Q. Q.; Tang, H.; Zhao, X. W. Insights into the Effect of Reactive Oxygen Species Regulation on Photocatalytic Performance via Construction of a Metal-Semiconductor Heterojunction. *J. Nanosci. Nanotechnol.* **2020**, *20*, 3478−3485.
(22) Sengupta, D. Effect of external field on bond energy and activation barrier for surface diffusion. *J. Cryst. Growth* **2006**, *286*, 91−95.
(23) Che, F. L.; Gray, J. T.; Ha, S.; McEwen, J. S. Improving Ni Catalysts Using Electric Fields: A DFT and Experimental Study of the Methane Steam Reforming Reaction. *ACS Catal.* **2017**, *7*, 551−562.
(24) Che, F.; Gray, J. T.; Ha, S.; McEwen, J. S. Catalytic water dehydrogenation and formation on nickel: Dual path mechanism in high electric fields. *J. Catal.* **2015**, *332*, 187−200.
(25) Stoukides, M. Electrochemical studies of methane activation. *J. Appl. Electrochem.* **1995**, *25*, 899−912.
(26) Jang, J.; Shen, K.; Morales-Guio, C. G. Electrochemical direct partial oxidation of methane to methanol. *Joule.* **2019**, *3*, 2589−2593.
(27) Che, F. L.; Ha, S.; McEwen, J. S. Elucidating the field influence on the energetics of the methane steam reforming reaction: A density functional theory study. *Appl. Catal., B* **2016**, *195*, 77−89.
(28) Che, F. L.; Gray, J. T.; Ha, S.; Kruse, N.; Scott, S. L.; McEwen, J. S. Elucidating the Roles of Electric Fields in Catalysis: A Perspective. *ACS Catal.* **2018**, *8*, 5153−5174.
(29) Huang, H.; Yu, Y.; Zhang, M. Mechanistic insight into methane dry reforming over cobalt: a density functional theory study. *Phys. Chem. Chem. Phys.* **2020**, *22*, 27320−27331.
(30) Baltrusaitis, J.; Jansen, I.; Schuttlefield Christus, J. D. Renewable energy based catalytic CH_4 conversion to fuels. *Catal. Sci. Technol.* **2014**, *4*, 2397−2411.
(31) Wang, Z.; Guo, M.; Baker, G. A.; Stetter, J. R.; Lin, L.; Mason, A. J.; Zeng, X. Methane-oxygen electrochemical coupling in an ionic liquid: a robust sensor for simultaneous quantification. *Analyst* **2014**, *139*, 5140−5147.
(32) Arnarson, L.; Schmidt, P. S.; Pandey, M.; Bagger, A.; Thygesen, K. S.; Stephens, I. E.; Rossmeisl, J. Fundamental limitation of electrocatalytic methane conversion to methanol. *Phys. Chem. Chem. Phys.* **2018**, *20*, 11152−11159.
(33) Arminio-Ravelo, J. A.; Escudero-Escribano, M. J. Strategies towards the sustainable electrochemical oxidation of methane to methanol. *Curr. Opin. Green. Sust.* **2021**, *30*, 100489.
(34) Xie, S.; Lin, S.; Zhang, Q.; Tian, Z.; Wang, Y. Selective electrocatalytic conversion of methane to fuels and chemicals. *J. Energy Chem.* **2018**, *27*, 1629−1636.
(35) Li, W.; He, D.; Hu, G.; Li, X.; Banerjee, G.; Li, J.; Lee, S. H.; Dong, Q.; Gao, T.; Brudvig, G. W.; Waegele, M. M.; Jiang, D. E.; Wang, D. Selective CO Production by Photoelectrochemical Methane Oxidation on TiO_2. *ACS Cent. Sci.* **2018**, *4*, 631−637.
(36) Wang, D.; Wang, H. F.; Hu, P. Identifying the distinct features of geometric structures for hole trapping to generate radicals on rutile TiO_2(110) in photooxidation using density functional theory calculations with hybrid functional. *Phys. Chem. Chem. Phys.* **2015**, *17*, 1549−1555.
(37) Wang, C. C.; Siao, S. S.; Jiang, J. C. C−H Bond Activation of Methane via σ−d Interaction on the IrO_2(110) Surface: Density Functional Theory Study. *J. Phys. Chem. C* **2012**, *116*, 6367−6370.
(38) Lien, C. F.; Chen, M. T.; Lin, Y. F.; Lin, J. L. Photooxidation of methane over TiO_2. *J. Chin. Chem. Soc.* **2004**, *51*, 37−42.
(39) Fung, V.; Tao, F. F.; Jiang, D. E. Low-temperature activation of methane on doped single atoms: descriptor and prediction. *Phys. Chem. Chem. Phys.* **2018**, *20*, 22909−22914.
(40) Yue, L.; Li, J.; Zhou, S.; Sun, X.; Schlangen, M.; Shaik, S.; Schwarz, H. Control of Product Distribution and Mechanism by Ligation and Electric Field in the Thermal Activation of Methane. *Angew. Chem., Int. Ed.* **2017**, *56*, 10219−10223.
(41) Van den Bossche, M.; Gronbeck, H. Methane Oxidation over PdO(101) Revealed by First-Principles Kinetic Modeling. *J. Am. Chem. Soc.* **2015**, *137*, 12035−12044.
(42) Zasada, F.; Janas, J.; Piskorz, W.; Gorczyńska, M.; Sojka, Z. Total Oxidation of Lean Methane over Cobalt Spinel Nanocubes Controlled by the Self-Adjusted Redox State of the Catalyst: Experimental and Theoretical Account for Interplay between the Langmuir−Hinshelwood and Mars−Van Krevelen Mechanisms. *ACS Catal.* **2017**, *7*, 2853−2867.
(43) Xu, B. B.; Zhou, M.; Zhang, R.; Ye, M.; Yang, L. Y.; Huang, R.; Wang, H. F.; Wang, X. L.; Yao, Y. F. Solvent Water Controls Photocatalytic Methanol Reforming. *J. Phys. Chem. Lett.* **2020**, *11*, 3738−3744.
(44) Zhang, J.; Peng, C.; Wang, H.; Hu, P. Identifying the Role of Photogenerated Holes in Photocatalytic Methanol Dissociation on Rutile TiO_2(110). *ACS Catal.* **2017**, *7*, 2374−2380.
(45) Henderson, M. A. A surface science perspective on TiO_2 photocatalysis. *Surf. Sci. Rep.* **2011**, *66*, 185−297.
(46) Di, J.; Yan, C.; Handoko, A. D.; Seh, Z. W.; Li, H.; Liu, Z. Ultrathin two-dimensional materials for photo- and electrocatalytic hydrogen evolution. *Mater. Today* **2018**, *21*, 749−770.
(47) Wang, D.; Sheng, T.; Chen, J.; Wang, H. F.; Hu, P. Identifying the key obstacle in photocatalytic oxygen evolution on rutile TiO_2. *Nat. Catal.* **2018**, *1*, 291−299.
(48) Dunnington, B. D.; Schmidt, J. R. Generalization of Natural Bond Orbital Analysis to Periodic Systems: Applications to Solids and Surfaces via Plane-Wave Density Functional Theory. *J. Chem. Theory Comput.* **2012**, *8*, 1902−1911.
(49) Glendening, E. D.; Landis, C. R.; Weinhold, F. Natural bond orbital methods. *Wiley Interdiscip. Rev.: Comput. Mol. Sci.* **2012**, *2*, 1−42.
(50) Dronskowski, R.; Blöchl, P. E. Crystal orbital Hamilton populations (COHP): energy-resolved visualization of chemical bonding in solids based on density-functional calculations. *J. Phys. Chem.* **1993**, *97*, 8617−8624.
(51) Valdes, A.; Qu, Z. W.; Kroes, G. J.; Rossmeisl, J.; Norskov, J. K. Oxidation and photo-oxidation of water on TiO_2 surface. *J. Phys. Chem. C* **2008**, *112*, 9872−9879.
(52) Tan, S.; Feng, H.; Ji, Y.; Wang, Y.; Zhao, J.; Zhao, A.; Wang, B.; Luo, Y.; Yang, J.; Hou, J. G. Observation of photocatalytic dissociation of water on terminal Ti sites of TiO_2(110)-1 × 1 surface. *J. Am. Chem. Soc.* **2012**, *134*, 9978−85.
(53) Kresse, G.; Hafner, J. Ab initio molecular dynamics for liquid metals. *Phys. Rev. B: Condens. Matter Mater. Phys.* **1993**, *47*, 558−561.
(54) Saitta, A. M.; Saija, F.; Giaquinta, P. V. Ab initio molecular dynamics study of dissociation of water under an electric field. *Phys. Rev. Lett.* **2012**, *108*, 207801.
(55) Zhang, L.; Mohamed, H. H.; Dillert, R.; Bahnemann, D. Kinetics and mechanisms of charge transfer processes in photo-

https://doi.org/10.1021/jacsau.1c00466
JACS Au 2022, 2, 188−196

catalytic systems: A review. *J. Photochem. Photobiol., C* **2012**, *13*, 263−276.
(56) Zhu, L. G.; Zhou, J.; Sun, Z. M. Reversible formation-dissociation of polaron in rutile driven by electric field. *Mater. Res. Lett.* **2018**, *6*, 165−170.

https://doi.org/10.1021/jacsau.1c00466
JACS Au 2022, 2, 188−196